京都大学防災研究所年報 第 54 号 A 平成 23 年 6 月
Annuals of Disas. Prev. Res. Inst., Kyoto Univ., No. 54 A, 2011

Catastrophic landslide induced by Typhoon Morakot, Shiaolin, Taiwan

Ching-Ying TSOU, Zheng-Yi FENG* and Masahiro CHIGIRA

* Department of Soil and Water Conservation, National Chung Hsing University, Taiwan

Synopsis

Typhoon Morakot induced the catastrophic and deadly Shiaolin landslide in southern Taiwan on 9 August 2009, resulting in more than 400 casualties. We undertook a geological and geomorphological investigation with the aim of reconstructing the events leading up to this landslide and to clarify factors that contributed to its development. The research results have been published with the title "Catastrophic landslide induced by Typhoon Morakot, Shiaolin, Taiwan" to the Journal of Geomorphology, volume 127, in 2011, where we provided the same contents as this paper. Cumulative rainfall reached up to 1676.5 mm in about three days under the influence of the typhoon, and the Shiaolin landslide, with a volume of 25×10^6 m^3, occurred one day after the peak in rainfall intensity. The landslide occurred on a dip slope overlying late Miocene to early Pliocene sedimentary rocks consisting of silty shale, massive mudstone, and sandstone. It started as a rockslide in the upper third of the landslide area and transformed into a rock avalanche that crossed a series of terraces and displaced or buried the village below. It buried the riverbed of the Chishan River and ran up the opposite slope, creating a landslide dam 60 m high, which was breached about 1 hour and 24 minutes later, flooding the village. The velocity of the landslide is estimated to have been 20.4 to 33.7 m s^{-1} and its apparent friction angle was 14°, which indicates its high mobility. The detachments in the source area consist of combinations of bedding planes and joints or faults. The landslide was preceded by gravitational deformation, which appeared as hummocky landforms before the landslide and as buckle folds exposed after the event. The landslide deposits consist of fragments of mudstone, shale, and sandstone, as well as clayey material at its base. This clayey material, consisting of illite, chlorite, quartz, feldspar, and calcite, is assumed to have strongly influenced the long, rapid runout.

Keywords: Typhoon Morakot, landslide, deep-seated landslide, gravitational slope deformation, Shiaolin

1. Introduction

A catastrophic landslide is a rapid, large gravitational mass movement, which changes the topography and remains for a long time. Guthrie and Evans (2007) regarded a landslide as catastrophic when it is individually formative and persist more than 10 times longer than moderate sized landslides. Many catastrophic landslides accompany avalanches—events that in their post-failure stage involve rapid runout and emplacement of relatively thin sheets of crushed, pulverized, and dry rock (Hewitt et al., 2008). Rock avalanche, which is also called sturzstrom (Heim,

1932; Hsü, 1975), may be complex as rockslide-avalanche (Mudge, 1965), or rockfall avalanche (Schuster and Krizek, 1978). Previous research on catastrophic landslides has been reviewed several times (Voight, 1978; Evans and DeGraff, 2002; Hewitt, 2006) and has shown that many are induced by earthquakes. Fewer cases have been reported of catastrophic landslides induced by rainstorms (Sidle and Chigira, 2004; Catane et al., 2007, 2008; Evans et al., 2007; Guthrie et al., 2009). In such cases, rock debris may be saturated with water (classified as debris flows) or not saturated (classified as debris avalanches) (Takahashi, 2010). One of the most recent catastrophic landslides occurred at Mt. Canabag in southern Leyte Island, Philippines, in 2006, which followed a continuous heavy rainfall and two recorded small earthquakes (Catane et al., 2007, 2008; Evans et al., 2007; Guthrie et al., 2009).

Catastrophic landslides are commonly preceded by gravitational deformation (Voight, 1978; Chigira, 1992, 2001; Chigira and Kiho, 1994; Evans and DeGraff, 2002; Crosta et al., 2006), although this by itself does not necessarily transform into catastrophic failure. The failure of slope is controlled by internal factors, such as fracture development in rock mass and external factors (Kilburn and Petley, 2003; Korup, 2004; Petley et al., 2005). Gravitational deformation creates a variety of internal structures and new materials (Hutchinson, 1988; Chigira, 1993a), some of which are more susceptible to earthquakes and others to rainstorms. Therefore, gravitational deformation may provide a clue in predicting potential sites of catastrophic landslides, and it must be interpreted in the context of slope development.

Progress in understanding these issues depends on the accumulation of case histories, particularly for contemporary landslides, as prehistoric landslides provide no direct information on their behavior and pre-event conditions. Here, we present the results of a geological and geomorphological investigation of the most recent rain-induced catastrophic landslide, which was triggered by Typhoon Morakot in Taiwan on 9 August, 2009.

Typhoon Morakot swept Taiwan on 7 August 2009, resulting in 619 deaths, 76 missing persons, the temporary evacuation of 24,950 residents, flooding, and more than US$ 5 billion in economic losses (National Disasters Prevention and Protection Commission, 2009). It also isolated numerous villages in southern mountain areas of Taiwan. It was the worst typhoon disaster in Taiwan for 50 years. The typhoon landed at Hualian in eastern Taiwan, crossed the island in a northwestward direction, and left at Taoyuan on the northwest coast (Fig. 1). The typhoon, which was a medium-strength event according to the classification system of the Taiwan Central Weather Bureau, with a maximum wind speed of 40 m s^{-1}, set a precipitation record of 2749 mm for a single rainfall event at Alishan, where the previous rainfall record of 1749 mm was set by Typhoon Herb in 1996 (Lin and Jeng, 2000).

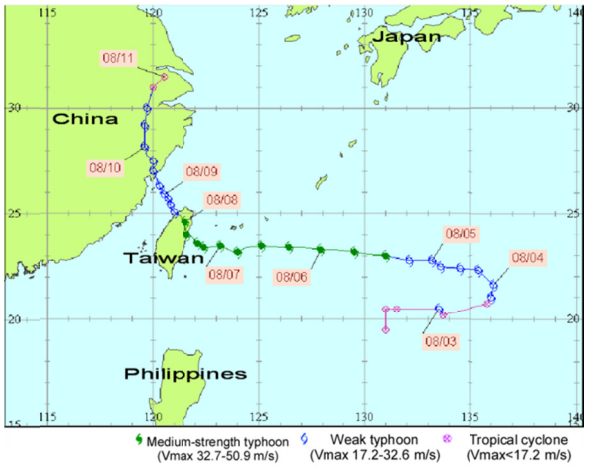

Fig. 1. Path of Typhoon Morakot (after Taiwan Central Weather Bureau, www.cwb.gov.tw).

The catastrophic landslide at Shiaolin Village, Kaohsiung County, was the largest landslide induced by Typhoon Morakot (Fig. 2). It occurred at 6:16 AM (local time) on 9 August, when the cumulative rainfall had reached 1676.5 mm, about three days after the start of rainfall according to the record at the Jiasian station (C0V250) of the Taiwan Central Weather Bureau, located 11.4 km SSW of the village (Fig. 3). The landslide dammed the rain-swollen Chishan River, but the dam was breached at about 7:40 AM on 9 August, flooding the downstream area (Feng, 2011). Abrupt river water level changes were recorded at 27.8 km downstream of Shiaolin Village (Feng, 2011): 2.75 m drop during the period from 7:10 to 7:50 AM and 7.88 m rise during the period from 8:40 to 9:30 AM.

Total casualties in Shiaolin Village were more than 400 people dead and missing. The village itself no longer exists.

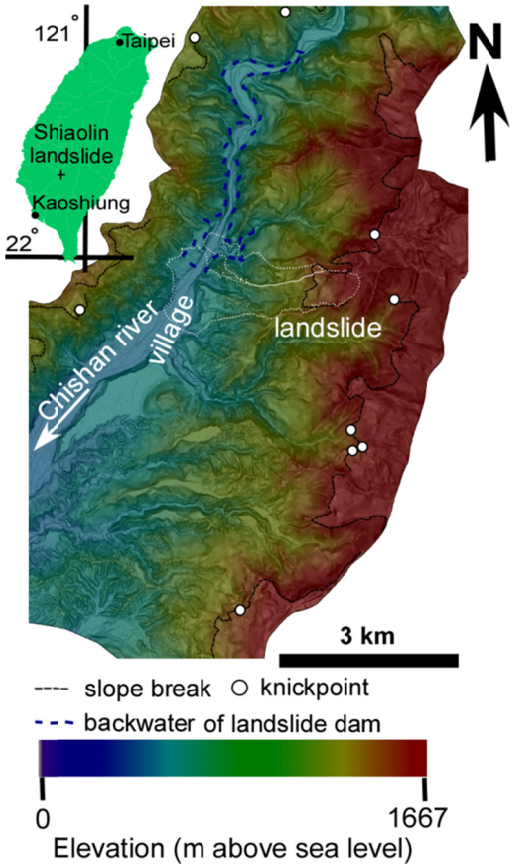

Fig. 2. Image map of the study area showing an elevation image superimposed on an inclination image. Low-relief surfaces occur at higher elevations, and terraces occur at lower elevations along the Chishan River. Small streams have knickpoints along the slope breaks. Formation of the landslide dam caused inundation of the area within 5 km upstream of the dam, as shown by the blue dashed line.

We investigated the Shiaolin landslide through fieldwork and analyses of digital elevation models (DEMs), topographic maps, rainfall data and seismic records, as well as analyses of mineralogy and particle size distribution of the landslide material. The main purposes of this study are: (I) to characterize the geological and geomorphological features of the Shiaolin landslide, (II) to describe the role of rainfall in this landslide and (III) to discuss whether it would have been possible to predict this landslide in advance.

2. Method

We conducted field investigations at two and seven months after the event, using a 1:10,000 scale topographic map that was magnified from a 1:25,000 scale map. We used a 5-m mesh DEM published by the Ministry of Interior of Taiwan to derive elevation and slope maps before the landslide. The Ministry constructed a new DEM after the event at the same resolution, which was used to analyze topographic changes. Rock-forming minerals were analyzed using an X-ray diffractometer (Rigaku Gaigerflex RAD IIB). Ethylene glycol treatment was used to identify clay minerals. We interpreted photographs downloaded from the Taiwan News website (www.etaiwannews.com) to examine the topography after the event and observed Google Earth imagery for the topography before the event. We referred to the information given by Takeshi Shibasaki of the Japanese broadcasting service Nippon Hoso Kyokai (NHK), who conducted thorough interviews with local residents, to reconstruct the landslide event. We used seismological data of two broadband stations of the Taiwan Central Weather Bureau: SGSB in Jiasian Township and TWMB in Chishan Township (11.4 km SSW and 47 km SSW from Shiaolin Village, respectively), to determine the timing and duration of the landslide event (Fig. 4). The distance between the landslide toe and the foot of source area (1.94 km) and the distance between the toe and the crown of the source area (3.2 km) were divided by the duration to estimate the landslide velocity. Precipitation was recorded at the Jiasian rainfall station (C0V250) (Fig. 4).

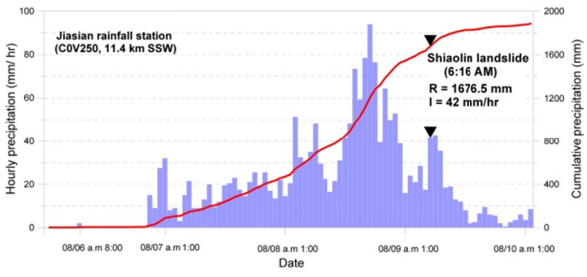

Fig. 3. Hourly and cumulative rainfall observed at Jiasian station (C0V250), 11.4 km SSW of the Shiaolin landslide (data from Taiwan Central Weather Bureau).

3. Geomorphological and geological setting

The region, located in the southern Western Foothills of Taiwan, is underlain by sedimentary rocks of Quaternary, Pliocene, and Miocene age (Fig. 4). The NE–SW-trending Neiying Fault, oriented parallel to the general strike of strata, runs across this area (Central Geological Survey, 2010a). The village was located on the valley floor on the left bank of the Chishan River, which flows southwestward in the mountains. Above the village was a 70-m-high terrace scarp with the terrace top at elevations of 400 to 450 m (Fig. 5). Terrace gravels were exposed in windows at the edge of the terrace after the landslide. Slopes above the terrace steepen to the east (from 15° to 78°) to reach a wide ridge of 700 to 1660 m in height, trending NNE–SSW with a low-relief top surface with slopes mostly less than 15°. The low-relief surface slopes to the west and terminates mainly at convex slope breaks. Small streams descending from the NNE–SSW-trending ridge have knickpoints along the slope breaks as shown in Fig. 2. The source area of the Shiaolin landslide is on a west-facing slope with elevations from 770 to 1280 m, at the rim of the low-relief surface. A small stream ran westward from a point at an elevation of 800 m before the landslide (Fig. 5), which became the foot of the source area of the landslide. The stream flow changed direction to northwestward at an elevation of 520 m and then to west-northwestward, dissecting the terrace. Pebble to cobble gravel beds were found to overlie mudstone at the elevation of 580 m on the E–W ridge, which indicates that the ridge was once a river terrace. The terrace surface, however, has been removed by erosion.

The Shiaolin landslide and subsequent flooding of the Chishan River stripped off vegetation and exposed new outcrops in a wide area. Consequently, the geologic map compiled during the present study improves upon the previous 1:50,000 scale geologic map, which was made from fewer outcrops by the Central Geological Survey, Ministry of Economic Affairs (Sung et al., 2000). The study area is underlain by the late Miocene to early Pliocene Yenshuikeng Formation (Sung et al., 2000), which consists of mudstone, sandstone, and shale (Fig. 6). The fresh sandstone is more strongly indurated than the mudstone and shale, and is estimated to have a uniaxial compressive strength of about 15 Mpa (Central Geological Survey, 2010b). The sandstone contains molds of dissolved shell fossils. The mudstone and shale include beds of siltstone and silty shale.

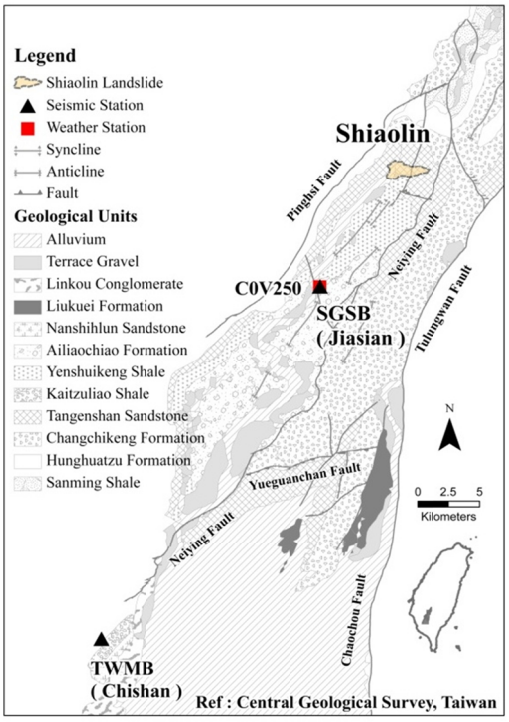

Fig. 4. Geologic outline map and locations of Jiasian weather station (C0V250) and seismic stations of the Taiwan Central Weather Bureau. Stations SGSB in Jiasian Township and TWMB in Chishan Township are within a region dominated by sedimentary rocks, based on a geologic map published by Central Geological Survey (2010a).

The geologic structure in and around the location of Shiaolin Village is characterized by an asymmetrical syncline whose axis trends NNE, plunges to the SSW, and runs to the east of the village. The beds on the west limb strike NE–SW and dip 30°–75° to the SE; the beds on the east limb strike NW–SE and dip 22°–48° to the SW. The source area of the landslide was the dip slope of the east limb of the syncline. This plunging syncline would show simple traces of strata on a horizontal cross-section, but because the strata and slopes on the east side of the Chishan River have similar attitudes, the bedding traces have rather complicated patterns. High-angle faults trending

NNE–SSW and E–W are found in the study area. An E–W-trending fault was exposed as the boundary of the southern margin of the landslide, and a NNE–SSW-trending fault bounded the eastern margin (Fig. 6). To the east of the NNE–SSW-trending fault, an NNE–SSW-trending anticline axis is shown in the 1:50,000 scale geologic map (Sung et al., 2000) outside the present study area.

4. Characteristics of the Shiaolin landslide

4.1 Morphology and deposits of the landslide

The Shiaolin landslide is 3.2 km long in an E–W direction and 0.8 to 1.5 km wide. The total fall height was 830 m from the top of the head scarp, at an elevation of 1280 m, to the toe of the landslide deposit at 450 m. The runout distance was about four times the total fall height, and its apparent friction angle, which is a parameter of landslide mobility, was 14°. A comparison of the topography before and after the landslide shows that the terrace above the village and the E–W-trending ridge to its northeast remained, and that the source area was the upper third of the landslide area. The source area is divided by the E–W-trending ridge into a larger southern part (source area A) and a smaller northern one (source area B) (Fig. 5a). The northern side of this ridge is cut by E–W-trending joints, as described below. The depth of the slide in the source area was estimated to be largely uniform, based on a comparison of DEM data before and after the event (Fig. 7). Calculations based on these DEMs indicate that the maximum depth of the landslide is 86.2 m in source area A and that the rock volume lost from source areas A and B was 25 $\times$ 10^6 m^3. Corresponding to the two source areas, the depositional area is also separated into two areas (areas A' and B') by the same ridge that bounds the two source areas (Fig. 5a).

Landslide deposits consist of blocks of sandstone, mudstone, shale, and dark clayey material containing mudstone fragments. The surfaces of landslide deposits displayed wrinkles, streaks of rock blocks of the same colors, and streaks of soil clods. Sandstone blocks of landslide deposits are larger than mudstone or shale blocks, with many being 2 to 5 m in diameter and a few as large as 10 m across. The deposits are topped with trees and grass, which are not mixed into the deposits even in the distal part across the Chishan River. The terrace surface above Shiaolin Village was covered by a layer of debris averaging 18 m in thickness, and the small valley was buried by debris to a maximum thickness of 82.5 m, so that only a small valley remained with its channel shifted about 50 m northward from its original location. Debris that covered Shiaolin Village was largely flushed away by surge waves after the dam breach, leaving landslide deposits mostly less than 10 m thick, topped with scattered large rock blocks. Landslide debris at the distal end across the Chishan River toppled trees forward and buried them. A N–S-trending linear step was found in these deposits 36 m from the landslide toe, which was 1 m high and 400 m long. This suggests that the deposits settled downhill after rushing up the slope.

The debris from source area A moved straight across the terrace surface or was deflected by a small mound at 580 m elevation and then descended the small valley dissecting the terrace, and swept across the Chishan River, forming a landslide dam. The debris from source area B moved northwestward to northward down a small valley, hit a spur projecting from the north side of the valley, and then changed direction to westward to reach the Chishan River. This distal part is assumed to have been thin and immersed in the lake behind the landslide dam.

4.2 Landslide dam

Substantial amounts of debris from source area A moved rapidly downhill to the west, burying the village, crossed the Chishan River and climbed 80 m up the opposite slope to an elevation of 460 m. Debris that was derived mainly from the small valley dissecting the terrace blocked the 80-m-wide river channel and formed a debris dam. From the topographic map and the DEMs, we estimate the landslide dam to have been 60 m high with its crest elevation at 435 m, which was the elevation of water marks in a house on the right bank of the river just upstream of the dam (Jia-Jyun Dong, pers. com.). Upstream from this dam, we observed signs of water on the slopes of both sides of the river: vegetation was draped on trees and grass was

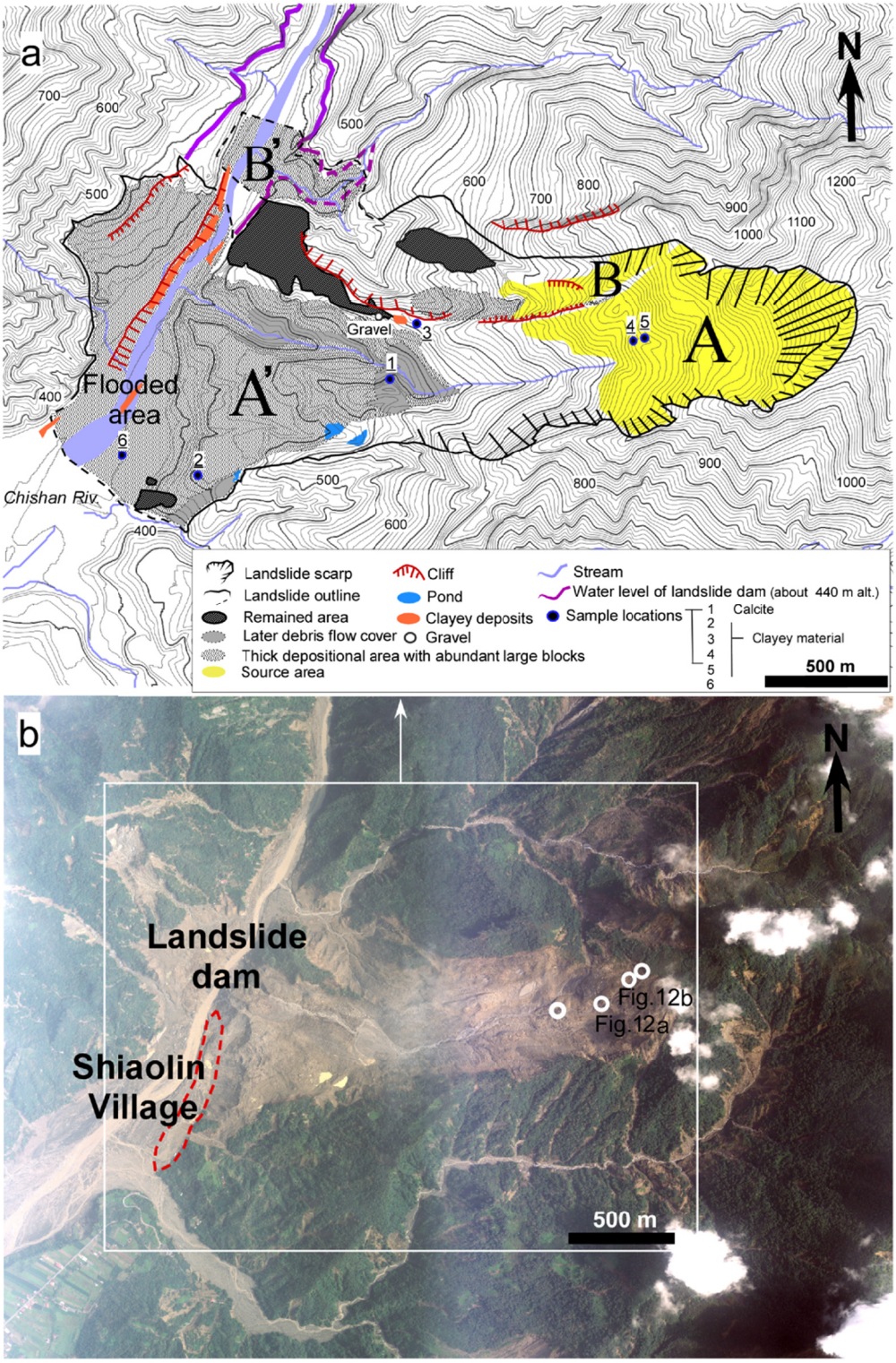

Fig. 5. Morphological features of the landslide and an aerial image of the area. (a) Morphological features of the landslide. The 10-m contours indicate the topography before the landslide. (b) Aerial image taken on 21 August 2009 by the Aerial Survey Office, Forestry Bureau, Taiwan. Circles indicate the locations of gravitationally deformed beds.

flattened. The backwater of the lake reached 5 km upstream from the dam, corresponding to a lake volume of 34.7×10^6 m^3 and a catchment area of 353.9 km^2. The internal structure of the dam was observed on the sides of its breach. The side on the right bank of the Chishan River contains a lower

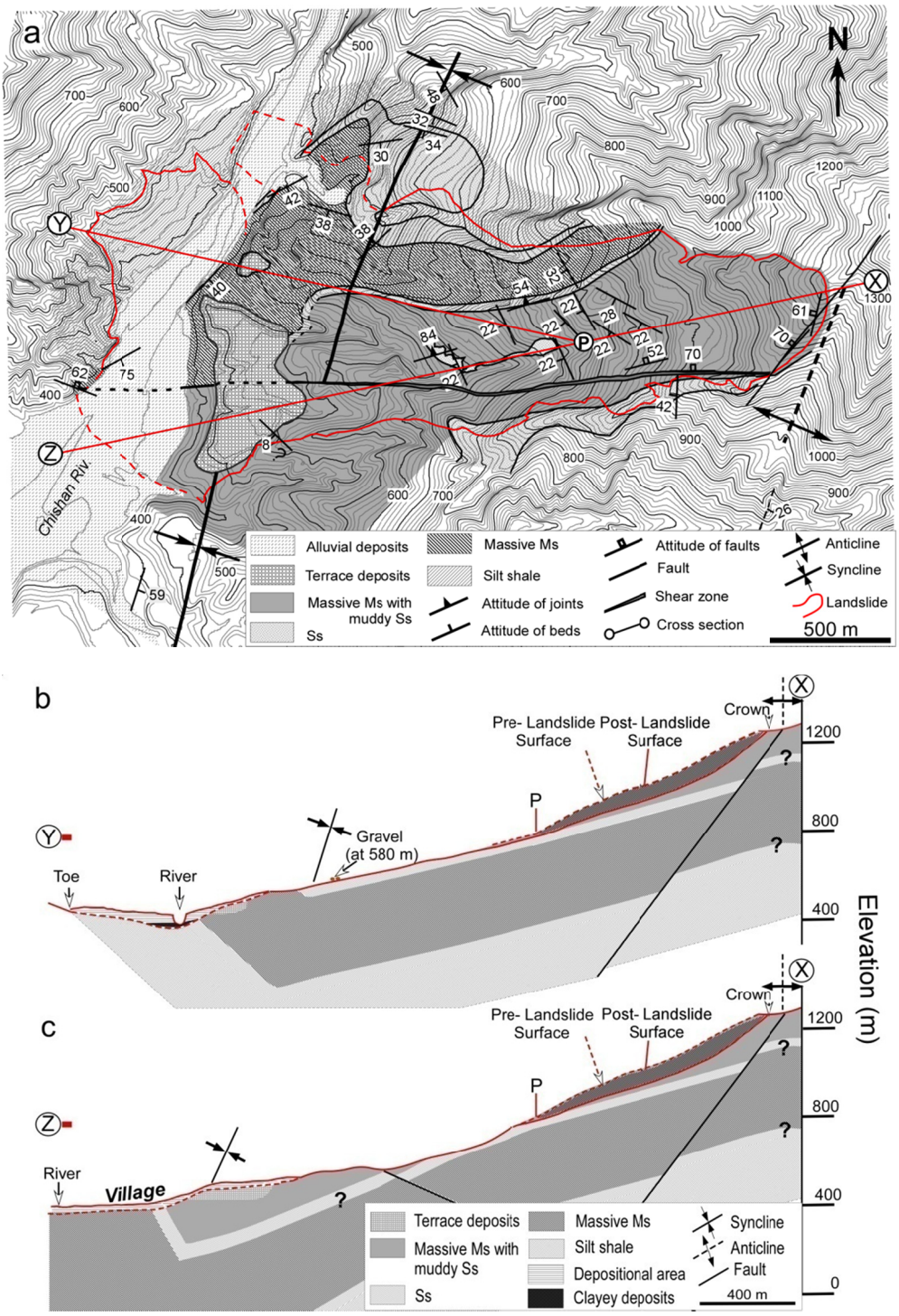

Fig. 6. Geologic map (10-m contours show the topography before the event) and cross-sections along slope lines. The distribution of geologic units within the landslide area has been reconstructed from data obtained after the landslide. Data on bedding and fault attitudes within the landslide area were measured after the event. Ms: mudstone; Ss: sandstone.

layer of dark gray clayey material and a 10-m-thick upper layer of rock blocks. The upper surface is covered by trees and grass. The landslide dam burst at 7:40 AM on 9 August (Feng, 2011), and the ensuing flood flushed away much of the downstream debris of the landslide.

4.3 Duration of the landslide event

The seismic waveforms induced by the Shiaolin landslide were recorded by broadband observatories.

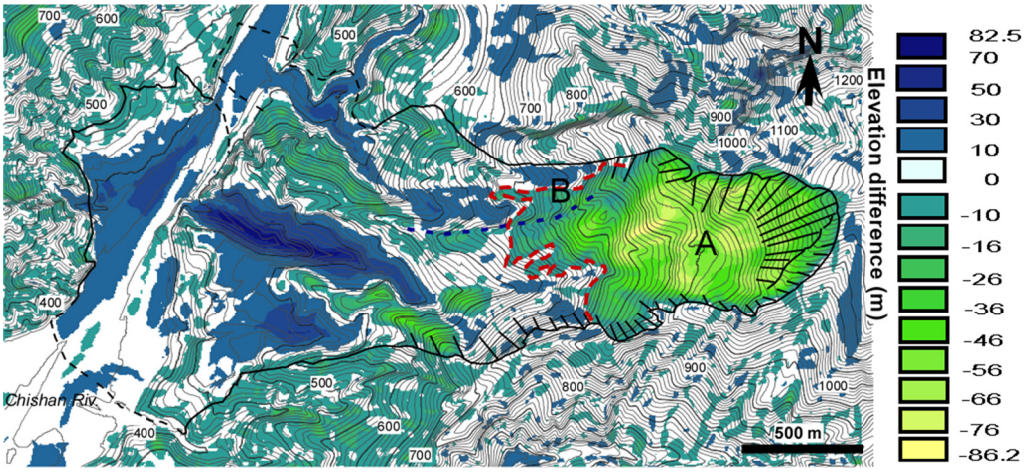

Fig. 7. Topography before and after the landslide event, derived from DEMs and a contour map published before the landslide. East–west-trending joints (blue dashed line) separate the source area into two parts. The base of the source area is indicated by the red dashed line.

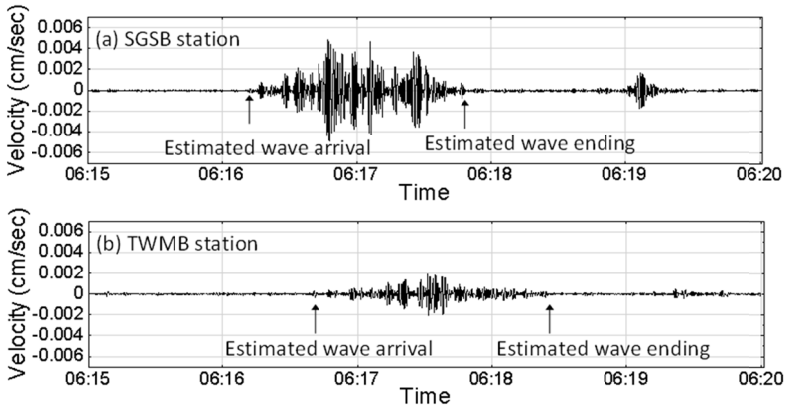

Fig. 8. The 5th intrinsic mode functions of the N–S velocity components of the signals recorded at stations SGSB and TWMB during 06: 15–06:20 AM on Aug. 9, 2009.

Records from two stations, SGSB at Jiasian and TWMB at Chishan, were selected for analysis in this study. Because Shiaolin Village lies along a sublinear NE–SW-trending line that also contains stations SGSB and TWMB, the N–S components of the two stations were analyzed. The signals are mixed with noise, especially the N–S velocity signal of station TWMB. We employed empirical mode decomposition (Huang et al., 1998; Crockett et al., 2010) to "sift" each N–S velocity signal into a set of intrinsic mode functions (IMFs), and we adopted the 5th IMFs of the signals at both stations (Fig. 8) for analysis of the wave propagation in this region. The seismic wave arrived at SGSB at approximately 6:16:15 AM and ended at 6:17:50 AM, which suggests that the landslide seismic signal lasted 95 s. The seismic wave arrived at station TWMB at 6:16:40 or 6:16:45 AM. Therefore, the travel time of the landslide wave between these two stations, 33 km apart, was 25–30 s. Because this line between the stations is dominated by sedimentary strata (Fig. 4) that strike subparallel to the line, we can assume a homogeneous medium and obtain a wave velocity of 1.1–1.32 km s^{-1}. Taking an average velocity of 1.21 km s^{-1} to represent the wave speed in this region and the distance between Shiaolin and station SGSB of 11.4 km, the travel time of the landslide wave was 9.4 s. This would put the start of the landslide at 6:16:06 AM, and this result is consistent with Lin et al (2010) and eyewitness accounts. From the vibration signal, the duration of the landslide was 95 s.

4.4 Geological structure and detachments

Source areas A and B are located on dip slopes on the east limb of the syncline. Source area A was occupied by massive mudstone with minor

sandstone and shale beds overlying a large sandstone bed, which is 30 m thick and was probably exposed along the stream bed before the landslide, because no elevation change occurred there (Figs. 7 and 9a). After the landslide, this sandstone was covered by shale and mudstone on the north side of the stream. It was newly exposed on the north side of the E–W-trending ridge (Fig. 9b), along E–W-trending en echelon joints dipping 54°–84° to the N (Fig. 9c). Planar sliding surfaces in shale located stratigraphically just above the thick sandstone are exposed in an area tens of meters across, beneath the debris in the middle and northern parts of source area A. An E–W-trending high-angle fault bounded the south rim of source area A (Fig. 9d), and an NNE–SSW-trending high-angle fault controlled the crown of this source area. Within source area B, sliding surfaces on shale below the thick sandstone bed and on another sandstone bed are exposed beneath debris. The detachment surfaces in source area B are this bedding plane in the north and the joints in the south, defining the E–W ridge. Bedding planes in source area A, which strike NW–SE and dip 28° to the SW, contain striations showing movement to the west (Fig. 10a). Westward or northwestward striations are developed on the joints bounding the south side of source area B (Fig. 10b).

4.5 Weathering

Calcite veins, which are commonly observed within the sandstone blocks of the deposits showed signs of dissolution in many blocks, being stained with iron precipitates (Fig. 11a). This is indicative that the calcite veins had already been dissolved before the landslide event. In addition, water flowing out of the source area precipitated calcite, which was identified by XRD analysis, on the bed of the stream in the depositional area after the event. This calcite occurred as thin films of pale yellow material (Fig. 11b). Calcite precipitation was recognized in many locations in the depositional

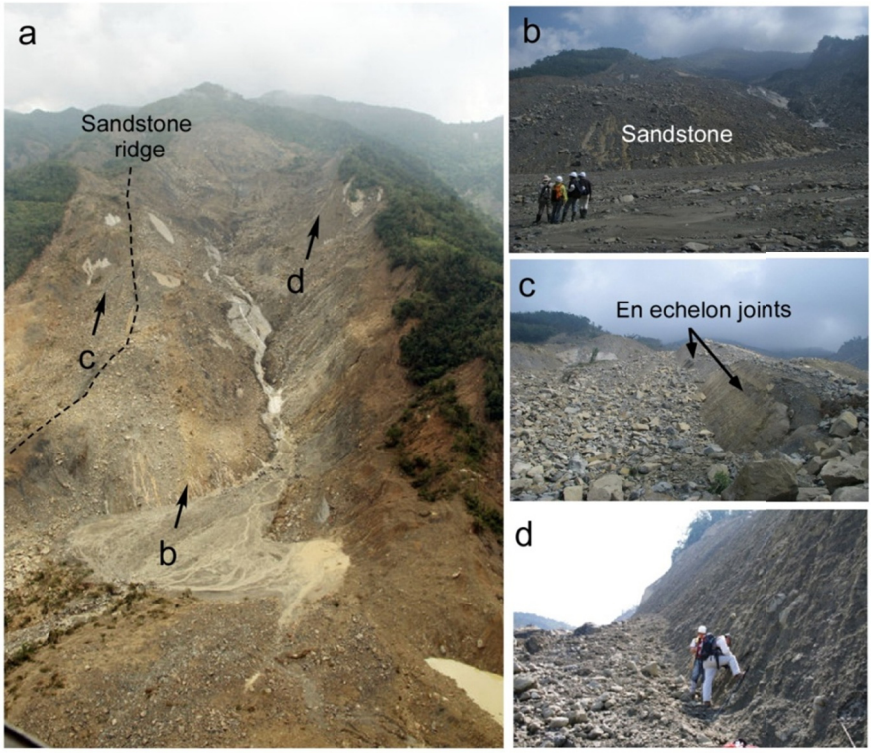

Fig. 9. Photographs of the landslide. (a) View of the upper two-thirds of the landslide. Dashed line indicates the E–W-trending sandstone ridge. Photo downloaded from Taiwan News (www.etaiwannews.com). The arrows indicate the direction of photographs b, c and d. (b) Sandstone bed that was probably exposed along the stream bed before the landslide occurred. (c) Detachment surfaces in source area B showing bedding planes in the north and E–W-trending en-echelon joints in the south. (d) East–west-trending high-angle fault bounding the southern margin of source area A. Rock debris on this surface adheres to fault gouge.

area and in the bed of the stream in the source area at its upstream end. Besides the pale yellow precipitates, white powdery precipitates occur on dry mudstone surfaces as weathering products. These were identified as thenardite (Na2SO4), gypsum (CaSO4· 2H2O), and halite (NaCl) by XRD analysis.

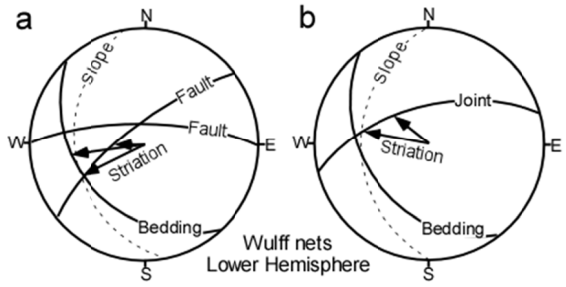

Fig. 10. Stereographic projections showing the orientations of bedding, faults, striations, and average slope attitude for (a) source area A and (b) source area B.

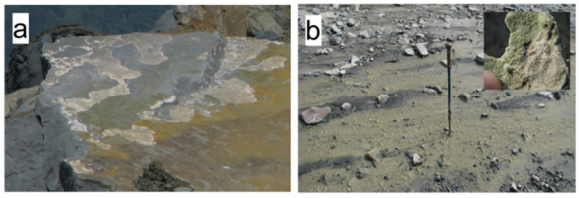

Fig. 11. Photographs of calcite veins and precipitation. (a) Calcite veins within sandstone blocks. (b) Calcite precipitated on the stream bed, deposited from water from the source area.

4.6 Gravitational slope deformation

Large volumes of destabilized material remained after the landslide in source areas A and B. In source area A, this material resembled debris, but we could recognize its continuity with previous bedding, particularly sandstone beds on the head scarp. The material was fractured but still maintained the morphology of beds. We found gravitationally deformed beds of alternating beds of sandstone and shale beneath this "debris" in at least four locations in the upper part of source area A. The beds were buckled, forming undulating beds or asymmetrical folds with a near-vertical downslope limb (Fig. 12). These buckle folds have limbs as long as 10 m. This deformation was accompanied by brittle fracturing and many fracture openings, particularly in sandstone beds, indicating that the deformation occurred near the ground surface.

Before the landslide, the slopes in the source area, where the buckle folds were found after the landslide, had hummocky rather than smooth surfaces, which are clearly identified on a Google earth image. Source areas A and B had irregularly shaped bulges and depressions, as shown in Fig. 13. These locations are related to the locations where buckle folds were found. We therefore assume the hummocky landforms to be the surface expression of gravitational deformation of the beds. Before the landslide, a stream emerged from the bottom of these hummocky slopes.

4.7 Characteristic and distribution of clayey material

At the base of the remaining debris in the lower part of source area A, there occurs dark-colored clayey material containing mudstone fragments (Fig. 14a). This material has chaotic texture and also fraction banding induced by shearing. The clayey material occurs in layers 1 to 2 m thick and consists of illite, chlorite, quartz, feldspar, and calcite, as identified by X-ray analysis. No swelling minerals were identified.

Dark clayey materials were found at the base of the deposits at the landslide dam site and in the depositional area usually as masses protruding from rock block debris. They are the same as those found in the source area, in terms of texture and mineralogy. These observations suggest that clayey materials form the basal part of the deposits. We observed the base of the deposits on the left bank of the Chishan River, where clayey material overlies alluvial gravel (Fig. 14b). The clayey material contains shear bands of up to 10 cm in thickness, in which platy rock fragments are aligned (Fig. 14c). The shear bands dip 36° to the S and are intercalated with weakly sheared zones that contain disintegrating mudstone blocks with "jigsaw structure".

5. Discussion

5.1 Geological causes of the landslide

We found that the orientation of the intersection lines of the en-echelon joints, high-angle fault, and bedding planes was the fundamental structural

cause of the Shiaolin landslide. The detachments consisted of bedding planes and high-angle faults in source area A, and bedding planes and en-echelon joints in source area B. The detachments exposed along the bedding planes are developed in shale next to thick sandstone beds, in both source areas. We found no bedding-parallel faults in the study area, but the beds are folded by a flexural slip mechanism, so bedding-parallel faults could have been produced by flexural slip along bedding planes that may have become a sliding surface of the landslide (Wang et al., 2003). The detachments bounding the south side of source areas A and B are a high-angle fault and en-echelon joints, respectively. The intersections of bedding planes and the faults or joints dip 27° and 25° respectively to the west, at a slightly lower angle than the surface slope; consequently, the intersection lines daylighted downslope (Fig. 10). Thus the orientation of these intersection lines was the fundamental structural cause of the landslide. In addition, the crown in source area A was controlled by an NE-trending fault.

Weathering, particularly dissolution of calcite, which is contained in rock matrices and veins, played a significant role in landslide initiation. The dissolution of calcite veins on the surfaces of rock blocks and iron staining along fractures increased fracture openings and separated blocks in the source area before the landslide occurred. The dissolution

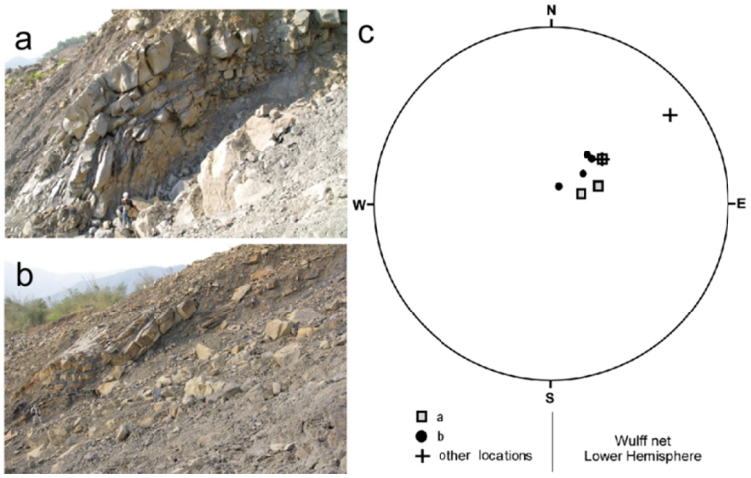

Fig. 12. Photographs of outcrops of the upper part of the landslide (a and b) and stereographic projection showing the orientation of folded beds (c). Buckle folds and abundant open fractures were observed in the rocks (see Figs. 5b and 13a for locations). The stereographic projection indicates that the folds have NW–SE-trending axes, indicative of movement to the SW.

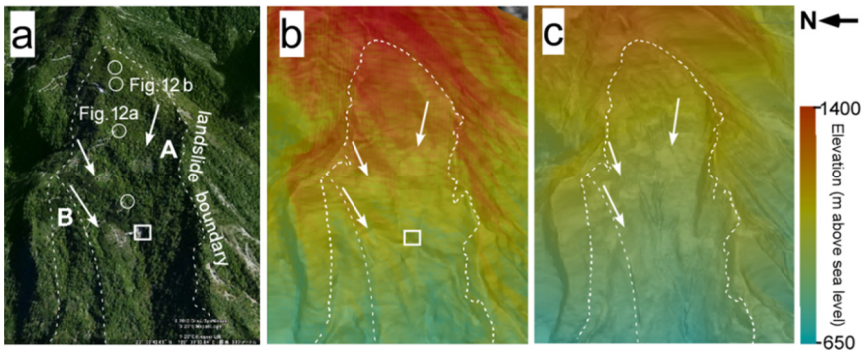

Fig. 13. Landforms in the source area before and after the landslide. (a) Google Earth image before the event. (b) Elevation image before the event, as constructed using a 5-m mesh DEM. (c) Elevation image after the event, as constructed using 5-m mesh DEM. Source area A had irregularly shaped bulges (arrows) and depressions, as shown in (a) and (b). Circles indicate the locations of gravitationally deformed beds (same locations as in Fig. 5b). Squares mark the source of a small stream before the landslide at an elevation of 800 m.

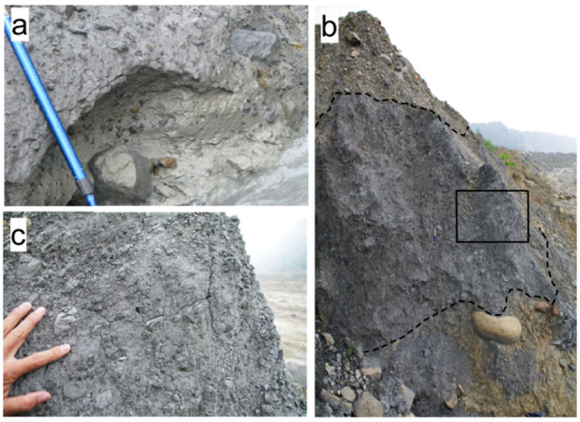

Fig. 14. Photographs of clayey material. (a) Dark clayey material consisting of fragments of mudstone; photograph taken near location 4 in Fig. 5a. (b) Clayey material overlying riverbed gravel and overlain by flood deposits. (c) Shear banding in clayey material in the squared area in (b). Shale fragments with aligned surfaces.

of the calcite veins can cause some large gaps in rock masses and subsequently induced excessive rainfall infiltration reaching the deep-seated failure surface. Chigira (1993b) performed weathering experiments on mudstone with calcite in the matrix and showed that calcite dissolution resulted in a significant decrease in shear strength.

5.2 Landslide velocity and mechanism

The velocity of the Shiaolin landslide was estimated at 20.4–33.7 m s^{-1} from seismic records and eyewitness accounts. These values are extremely high in comparison with debris flows in Jiangjia Gully, China, which typical viscous debris flows, for which frontal velocities range from 6–10 m s^{-1} (Takahashi, 2010). The apparent friction angle of the highly mobile Shiaolin landslide was 14°, a 0.25 equivalent coefficient of friction (Fig. 15). Debris volume of a rock avalanche is inversely proportional to the apparent friction angle (Hsü, 1975; Okuda, 1984). The Shiaolin landslide is consistent with this trend (Fig. 15).

The rapid movement of the Shiaolin landslide could be explained by its mechanism of movement. Rock avalanches do not require materials that are saturated with water and may occur in partially to completely unsaturated materials, so different mechanisms have been proposed from those of water-saturated debris flows, including grain collision (Heim, 1932), fluidization (Kent, 1966), air-layer lubrication (Shreve, 1966), pressure from vaporized pore water (Goguel, 1978), and acoustic fluidization (Melosh, 1979). However, most studied rock avalanches have been induced by earthquakes, and few rock avalanches have been reported to be induced by rainfall.

The Shiaolin landslide, which was induced by a rainstorm, has clayey material with blocks of sandstone, mudstone, and shale. This clayey material, which is assumed to be made by shearing during the landslide movement as well as by earlier gravitational deformation, forms an essentially impermeable layer at the base of the landslide material, suggesting that heavy rainfall penetrates downward to the layer of clayey material, where water pressure builds up and decreases the effective

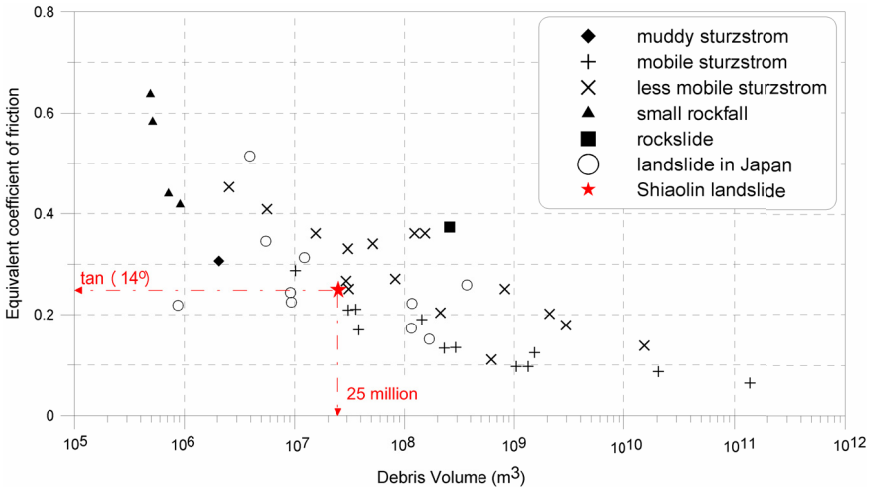

Fig. 15. Comparison of the relation between debris volume and apparent friction for the Shiaolin landslide and large landslides in the world (Hsü, 1975) and Japan (Okuda, 1984).

stress. This could have been the trigger of the initiation of the Shiaolin landslide. After the initiation of the movement, the clayey material probably played an important role to form a lubricating layer at the base of landslide material by keeping high pore pressure during movement. This phenomenon has been investigated in flume tests, which show that the pore pressure increases rapidly with increasing fine-grained content and movement velocity during shearing (Wang and Sassa, 2003). Evans et al. (2007) attributed the long runout of the Leyte landslide, the Philippines, to the loading of undrained paddy field material in the path of the landslide.

5.3 Role of rain in this event

The Shiaolin landslide occurred about 1 day after the peak of rainfall intensity, which could be attributable to the infiltration behavior of rainwater through the gravitationally deformed rock body. The source area of the Shiaolin landslide had been gravitationally deformed beforehand, which suggests that the deformed rock body was fractured and permeable, except for the essentially impermeable clayey material and intact rock. Fractures have the potential to become pathways for water infiltration that would cause water pressure buildup at depth. In contrast to the Shiaolin landslide, many shallow landslides occurred when rainfall intensity was increasing or near its peak (Godt et al., 2006; Yu et al., 2006). This difference in terms of landslide timing is attributed to the difference in the effects of water infiltration and pore water pressure buildup. A time lag between peak rainfall intensity and landslide initiation is commonly observed for large landslides (Lollino et al., 2006; Evans et al., 2007; Chigira, 2009), considered to reflect the time required for water infiltration to deep levels. Rapid infiltration in shallow soil layers means that pore water pressure responds to rainfall quickly and landslides occur when rainfall intensity is strong.

We suggest the geological, geomorphological conditions, and landslide type needs to be taken into account when evaluating the susceptibility of a location to rain-induced landsliding in addition to the variables of rainfall, such as the combination of rainfall intensity and duration (Caine, 1980; Guzzetti et al., 2008) or the combination of mean and maximum hourly intensity, duration, and rainfall amount (Dhakal and Sidle, 2004).

5.4 Prediction of the Shiaolin landslide site

Can the site of the Shiaolin landslide be predicted beforehand? We believe that this site could be extracted as a potential site based on the unusual landform before the event. The hummocky slope morphology was easily identified on the Google earth image before the event as stated before and it could have been delineated more clearly by using aerial photographs, which have much higher resolution than the Google earth image. Internal structure of the hummocky slopes, which have been identified as gravitational buckle folds with many openings after the event, might not have been found before the event, but the geological map made by the Central Geological Survey (Sung et al., 2000) indicated that the source area are located on a dip slope notwithstanding that the detailed distribution of beds was not precise. On a dip slope, buckle folds is one of the common gravitational deformation types as well as sliding (Chigira, 2001) and are highly unstable and easily transform into catastrophic failure, because when the downslope limb of a buckle fold is removed, the upslope limb loses its support from downslope and becomes suddenly destabilized (Wang et al., 2003; Tommasi et al., 2009).

Gravitational slope deformation develops and leads to a catastrophic landslide at a certain condition, so we need to pick up a gravitational slope deformation just before the catastrophic event from various stages of gravitational slope deformation. Moriwaki (2001) performed a statistical analysis of various field monitoring and experimental data on landslides and found that there is a critical strain, which is defined as the ratio between a slope displacement at its upper part and the slope length just before landsliding. According to Chigira (2009), this ratio is consistent with the ratio between the length of a scarplet and the length of a gravitationally deformed slope. Chigira (2009) also analyzed large landslides induced by a rainstorm and found that they were preceded by gravitational deformation and that their “strains” were as small as 1 to 16% before the event and

interpreted that they were under the critical strain just before the failure. These ideas of critical strain may be similar to those found by Saito and Uezawa (1966), Fukuzono (1985), Voight (1988), and Petley and Allison (1997). Whether the gravitational deformation at the Shiaolin landslide site had been at a critical condition or not could be examined by using high-resolution aerial photographs, which were not available. In addition we need further research to examine whether there were such potential sites near the Shiaolin landslide site or not by using aerial photographs.

The gravitational slope deformation that preceded the Shiaolin landslide were located at the margin of a low-relief surface, which suggests that the gravitational deformation leading to catastrophic landslide can be interpreted and located from the view point of long-term slope development. The paleosurface, the age of which is unknown, has been dissected by the rejuvenation of the Chishan River and its tributaries in response to base-level lowering associated with tectonic uplift of the area. Corresponding to the incision, the walls of the river valley have been denudated by mass movements, which possibly started as gravitational slope deformation in areas with adverse geological structures as a precursory stage of landslide. During this dissection, the valley walls were debuttressed and destabilized by undercutting. This idea can also be linked to the notion of 'waves of aggression' in landscape (Brunsden, 2001). Such a combination of slope development, gravitational deformation, and landslide occurrence was reported in nonglaciated areas such as Kyushu in Japan (Chigira, 2009). The effect of debuttressing on slope destabilization is expected to be similar but less severe than that of glaciated valleys in Europe and North America (Bovis and Evans, 1996; Arsenault and Meigs, 2005; Ambrosi and Crosta, 2006; Brückl and Brückl, 2006), initiating gravitational deformation of slopes, destabilization, and failure during severe rainstorms or snow melting (Crosta et al., 2006).

6. Conclusions

We investigated the geological and geomorphological features of the catastrophic 2009 Shiaolin landslide, which was induced by a cumulative rainfall of 1676.5 mm by Typhoon Morakot and buried Shiaolin Village. The landslide occurred on a dip slope in late Miocene to early Pliocenesedimentary rocks consisting of shale, massive mudstone, and sandstone. The source area was the slope that had been gravitationally deformed beforehand. The deformation appeared as a hummocky slope surface before the event and was observed as gravitational buckle folds in the source area after the event. Gravitational deformation occurred with a preferable geological structure of wedge-shaped detachments consisting of bedding planes and joints or fault planes. Gravitational deformation occurred at the margin of a low-relief paleosurface, the apparent result of denudation of this surface. The gravitationally deformed rocks were not only mechanically but also chemically deteriorated, as suggested by large amounts of calcite precipitation from water draining from the source area. Thus, structural factors, weathering, and gravitational slope deformation were the underlying causes of the landslide. The landslide deposit consisted of a thin sheet of debris consisting of rock blocks and pulverized rock with weak clayey material at their base. This clayey material, which was probably produced by shearing during the landslide movement as well as earlier gravitational deformation, must have played an important role in the long, rapid runout by pressure build up and its persistence.

Acknowledgements

We thank professors Su-Chin Chen of National Chung Hsing University, Gonghui Wang of Kyoto University and Jia-Jyun Dong of National Central University for useful discussion. Mr. Takeshi Shibasaki of NHK provided details on eyewitness accounts. Broadband seismic data from stations SGSB and TWMB and rainfall data were kindly supplied by the Central Weather Bureau of Taiwan. We are grateful to Dr. Takashi Oguchi and anonymous referees whose comments improved the paper. This study was partly supported by the Interchange Association, Japan, a Sasakawa Scientific Research Grant, and the National Science Foundation of Taiwan (NSC-97-2313-B-005-042-MY3).

References

Ambrosi, C., Crosta, G.B. (2006): Large sackung along major tectonic features in the Central Italian Alps, Engineering Geology, Vol. 83, No.1-3, pp. 183–200.

Arsenault, A.M., Meigs, A.J. (2005): Contribution of deep-seated bedrock landslides to erosion of a glaciated basin in southern Alaska, Earth Surface Processes and Landforms, Vol. 30, No. 9, pp. 1111-125.

Bovis, M.J., Evans, S.G. (1996): Extensive deformations of rock slopes in southern Coast Mountains, Southwest British Columbia, Canada, Engineering Geology, Vol. 44, No. 1-4, pp. 163-82.

Brückl, E., Brückl, J. (2006): Geophysical models of the Lesachriegel and Gradenbach deep-seated mass-movements (Schober range, Austria), Engineering Geology, Vol. 83, No. 1-3, pp. 254–272.

Brunsden, D. (2001): A critical assessment of the sensitivity concept in geomorphology, Catena, Vol. 42, No.2-4, pp. 99–123.

Caine, N. (1980): The rainfall intensity-duration control of shallow landslides and debris flows, Geografiska Annaler. Series A. Physical Geography, Vol. 62, No. 1-2, pp. 23-27.

Catane, S.G., Cabria, H.B., Tomarong, C.P., Saturay, R.M., Zarco, M.A.H., Pioquinto, W.C. (2007): Catastrophic rockslide-debris avalanche at St. Bernard, Southern Leyte, Philippines, Landslides, Vol. 4, No. 1, pp. 85-90.

Catane, S.G., Cabria, H.B., Zarco, M.A.H., Saturay, R.M., Mirasol-Robert, A.A. (2008): The 17 February 2006 Guinsaugon rock slide-debris avalanche, Southern Leyte, Philippines: deposit characteristics and failure mechanism, Bulletin of Engineering Geology and the Environment, Vol. 67, No. 3, pp. 305-320.

Central geological Survey (2010a): Query system of topographic and geological databases for watersheds. Available at http://gwh.moeacgs.gov.tw/gwh/gsb97-2/sys9/ (in Chinese).

Central geological Survey (2010b): Query system of environmental geological hazard. Available at http://envgeo.moeacgs.gov.tw/ (in Chinese).

Chigira, M. (1992): Long-term gravitational deformation of rocks by mass rock creep, Engineering Geology, Vol. 32, No. 3, pp. 157-184.

Chigira, M. (1993a): Basic geologic causes of Aka-kuzure. Landslide News, Vol. 7, pp. 14-15.

Chigira, M. (1993b): Dissolution and oxidation of mudstone under stress, Canadian Geotechnical Journal, Vol. 30, No. 1, pp. 60-70.

Chigira, M. (2001): Geological structures of large landslides in Japan, Journal of Nepal Geological Society, Vol. 22, pp. 497-504.

Chigira, M. (2009): September 2005 rain-induced catastrophic rockslides on slopes affected by deep-seated gravitational deformations, Kyushu, southern Japan, Engineering Geology, Vol. 108, No. 1-2, pp. 1-15.

Chigira, M., Kiho, K. (1994): Deep-seated rockslide-avalanches preceded by mass rock creep of sedimentary-rocks in the Akaishi Mountains, Central Japan, Engineering Geology, Vol. 38, No. 3-4, pp. 221-230.

Crockett, R.G.M., Perrier, F., Richon, P. (2010): Spectral-decomposition techniques for the identification of periodic and anomalous phenomena in radon time-series, Natural Hazards and Earth System Sciences, Vol. 10, No. 3, pp. 559-564.

Crosta, G.B., Chen, H., Frattini., P. (2006): Forecasting hazard scenarios and implications for the evaluation of countermeasure efficiency for large debris avalanches, Engineering Geology, Vol. 83, No. 1-3, pp. 236-253.

Dhakal, A.S., Sidle, R.C. (2004): Distributed simulations of landslides for different rainfall conditions, Hydrological Processes, Vol. 18, No. 4, pp.757-776.

Evans, S.G., DeGraff, J.V. (2002): Catastrophic landslides: effects, occurrences and mechanisms, In: S.G. Evans and J.V. DeGraff (Editors), Reviews in Engineering Geology, Vol. 15. Geological Society of America, pp. 411.

Evans, S.G., Guthrie, R.H., Roberts, N.J., Bishop, N.F. (2007): The disastrous 17 February 2006 rockslide-debris avalanche on Leyte Island, Philippines: a catastrophic landslide in tropical mountain terrain, Natural Hazards and Earth System Sciences, Vol. 7, No.1 , pp.89-101.

Feng, Z.Y. (2011): The seismic signatures of the 2009 Shiaolin landslide in Taiwan, Natural Hazards and Earth System Sciences, Vol. 11, No. 5, pp. 1559-1569.
Fukuzono, T. (1985): A new method for predicting the failure time of slope, Proc. of 4th I.S.L., Tokyo, 145-150.
Godt, J.W., Baum, R.L., Chleborad, A.F. (2006): Rainfall characteristics for shallow landsliding in Seattle, Washington, USA, Earth Surface Processes and Landforms, Vol. 31, No. 1, pp. 97-110.
Goguel, J. (1978): Scale-dependent rockslides mechanisms, with emphasis on the role of pore fluid vaporization, In: B. Voight (Editor), Rockslides and Avalanches, Developments in Geotechnical Engineering, 14A. Elsevier, New York, pp. 693-705.
Guthrie, R.H., Evans, S.G. (2007): Work, persistence, and formative events: The geomorphic impact of landslides, Geomorphology, Vol. 88, No. 3-4, pp. 266-275.
Guthrie, R.H., Evans, S.G., Catane, S.G., Zarco, M.A.H., Saturay, R.M. (2009): The 17 February 2006 rock slide-debris avalanche at Guinsaugon Philippines: a synthesis, Bulletin of Engineering Geology and the Environment, Vol. 68, No. 2, pp. 201-213.
Guzzetti, F., Peruccacci, S., Rossi, M., Stark, C.P. (2008): The rainfall intensity-duration control of shallow landslides and debris flows: an update, Landslides, Vol. 5, No. 1, pp. 3-17.
Heim, A. (1932): Bergstürz und Menschenleben, Fretz and Wasmutb, Zürich, 218 pp.
Hewitt, K. (2006): Disturbance regime landscapes: mountain drainage systems interrupted by large rockslides, Progress in Physical Geography, Vol. 30, No. 3, pp. 365-393.
Hewitt, K., Clague, J.J., Orwin, J.F. (2008): Legacies of catastrophic rock slope failures in mountain landscapes, Earth-Science Reviews, Vol. 87, No. 1-2, pp. 1-38.
Hsü, K.J. (1975): Catastrophic debris streams (sturzstroms) generated by rockfalls, Geological Society of America Bulletin, Vol. 86, No. 1, pp. 129-140.
Huang, N.E., Shen, Z., Long, S.R., Wu, M.C., Shih, H.H., Zheng, Q., Yen, N.C., Tung, C.C., Liu, H.H. (1998): The empirical mode decomposition and the Hilbert spectrum for nonlinear and non-stationary time series analysis, Proceedings of Royal Society of London Series A 454, 903-995.
Hutchinson, J.N. (1988): General report: morphological and geotechincal parameters of landslides in relation to geology and hydrology, Proceedings, 5th International Symposium on Landslides, Lausanne, Switzerlan, pp. 3-35.
Kent, P.E. (1966): The transport Mechanism in Catastrophic Rock Falls, Journal of Geology, Vol. 74, No. 1, pp. 79-83.
Kilburn, C.R.J., Petley, D.N. (2003): Forecasting giant, catastrophic slope collapse: lessons from Vajont, Northern Italy, Geomorphology, Vol. 54, No. 1-2, pp. 21-32.
Korup, O. (2004): Geomorphic implications of fault zone weakening: slope instability along the Alpine Fault, South Westland to Fiordland, New Zealand Journal of Geology and Geophysics, Vol. 47, No. 2, pp. 257-267.
Lin, M.L., Jeng, F.S. (2000): Characteristics of hazards induced by extremely heavy rainfall in Central Taiwan -Typhoon Herb, Engineering Geology, Vol. 58, No. 2, pp. 191-207.
Lin, C.H., Kumagai, H., Ando, M., Shin, T.C. (2010): Detection of landslides and submarine slumps using broadband seismic networks, Geophysical Research Letters, Vol. 37, No. L22309, doi:10.1029/2010gl044685.
Lollino, G., Arattano, M., Allasia, P., Giordan, D. (2006): Time response of a landslide to meteorological events, Natural Hazards and Earth System Sciences, Vol. 6, No. 2, pp. 179-184.
Melosh, H.J. (1979): Acoustic fluidization- a new geologic process?, Journal of Geophysical Research, Vol. 84, No. B13, pp. 7513-7520.
Moriwaki, H. (2001): A risk evaluation of landslides in use of critical surface displacement. Landslides - Journal of the Japan Landslide, Society, Vol. 38, No. 2, pp. 115-122 (in Japanese, with English Abstract).
Mudge, M.R. (1965): Rockfall-avalanche and Rockslide-avalanche deposits at Sawtooth ridge, Montana, Geological Society of America Bulletin, Vol. 76, No. 9, pp. 1003-1014.
National Disasters Prevention and Protection Commission, R.O.C. (2009): Typhoon Morakot

Disaster Responses Reports from Typhoon Morakot Central Emergency Operating Center 74th Report, Available at http://www.nfa.gov.tw/upload/content/2009/20090909/2009998323063.pdf

Okuda, S. (1984): Features of debris deposits of large slope failures investigated from historical records, Disaster Prevention Research Institute. Annuals 27 (B-1), pp. 353-468 (in Japanese, with English Abstract).

Petley, D.N., Allison, R.J. (1997): The mechanics of deep-seated landslides, Earth Surface Processes and Landforms, Vol. 22, No. 8, pp. 747-758.

Petley, D.N., Higuchi, T., Petley, D.J., Bulmer, M.H., Carey, J. (2005): Development of progressive landslide failure in cohesive materials, Geology, Vol.33, No. 3, pp. 201-204.

Saito, M., Uezawa, H. (1966): Forecasting the time of occurrence of a slope failure, Journal of Japanese Landslide Society, Vol. 2, No. 2, pp. 7-12 (in Japanese).

Schuster, R.L., Krizek, R.J. (1978): Landslides: Analysis and Control, Special Report, Transportation Research Board, National Academy of Sciences, 176. National Academy of Sciences, Washington, DC, pp. 234.

Shreve, R.L. (1966): Sherman landslide Alaska, Science, Vol.154, No. 3757, pp. 1639-643.

Sidle, R.C., Chigira, M. (2004):. Landslides and debris flows strike Kyushu, Japan, EOS, Vol. 85, No. 15, pp. 145-51.

Sung, Q.C., Lin, C.W., Lin, W.H., Lin, W.C. (2000): Explanatory text of the geologic map of Taiwan, Chiahsien sheet, scale 1/50,000, Central Geological Survey, Ministry of Economic Affairs, Taiwan, 57 pp.

Takahashi, T. (2010): Debris flow: mechanics, prediction and countermeasures, Taylor and Francis, London, 448 pp.

Tommasi, P., Verrucci, L., Campedel, P., Veronese, L., Pettinelli, E., Ribacchi, R. (2009): Buckling of high natural slopes: The case of Lavini di Marco (Trento-Italy), Engineering Geology, Vol. 109, No. 1-2, pp. 93-08.

Voight, B. (1978): Lower Gros Ventre slide, Wyoming, U.S.A. In: B. Voight (Editor), Rockslides and avalanches, Elsevier, Amsterdam, pp. 113-60.

Voight, B. (1988): A method for prediction of volcanic eruptions, Nature, Vol. 332, No. 6160, pp.125-30.

Wang, G.H., Sassa, K. (2003): Pore-pressure generation and movement of rainfall-induced landslides: effects of grain size and fine-particle content, Engineering Geology Vol. 69, No. 1-2, pp.109-125.

Wang, W.N., Chigira, M., Furuya, T. (2003): Geological and geomorphological precursors of the Chiu-fen-erh-shan landslide triggered by the Chi-chi earthquake in central Taiwan, Engineering Geology Vol. 69, No. 1-2, pp. 1-13.

Yu, F.C., Chen, T.C., Lin, M.L., Chen, C.Y., Yu, W.H. (2006): Landslides and rainfall characteristics analysis in Taipei City during the Typhoon Nari event, Natural Hazards, Vol. 37, No. 1-2, pp.153-167.

2009 年台風モラコットによる台湾の深層崩壊災害

鄒青穎・馮正一*・千木良雅弘

*台湾国立中興大学水土保持学系

要　旨

台湾南部の小林村は2009年8月9日に台風莫拉克（Morakot）によって深刻な崩壊がもたらされ，400人以上の死者が出た。三日間の累計降雨量は1676.5㎜に達し，降雨強度のピークを迎えた翌日に崩壊が発生した。今回の崩壊は流れ盤に起こり，崩壊体積は25×10^6㎥に及んだ。その基盤は中新世後期から鮮新世前期にかけて形成した堆積岩であり，シルト頁

岩，厚い泥岩と砂岩を含有する。大規模な斜面崩壊土が旗山川の谷を塞ぎ，向かい側の急斜面上に広がりながら，村の上流に高さ60mの天然ダムを形成した。天然ダムは形成後の1時間24分後に崩壊した。崩壊の移動速度は約20.4～33.7ms^{-1}と推定され，また，見かけ摩擦角度は14°であった。崩壊源のディタッチメントは層理，節理及び断層であった。崩壊源の地層は重力変形を受けており，崩壊前には不規則な凹凸の地形を示していた。また，この地層の重力変形は崩壊後に座屈変形として確認された。崩壊の堆積物は泥岩，頁岩および砂岩などの岩屑を含有し，底部には広く粘度が認められ，それはイライト，緑泥石，石英，長石および方解石からなっていた。この粘度が高速かつ長距離の移動の大きな要因となったと推定される。

キーワード：台風モラコット，豪雨，地すべり，深層崩壊，重力斜面変形，小林村